ACS APPLIED MATERIALS & INTERFACES

Research Article

www.acsami.org

Growth Kinetics and Growth Mechanism of Ultrahigh Mass Density Carbon Nanotube Forests on Conductive Ti/Cu Supports

Hisashi Sugime,*[,†] Santiago Esconjauregui,[†] Lorenzo D'Arsié,[†] Junwei Yang,[†] Taron Makaryan,[†,‡] and John Robertson[†]

[†]Department of Engineering, University of Cambridge, Cambridge CB3 0FA, United Kingdom

[‡]Faculty of Radiophysics, Yerevan State University, Yerevan 0005, Armenia

ABSTRACT: We evaluate the growth kinetics and growth mechanism of ultrahigh mass density carbon nanotube forests. They are synthesized by chemical vapor deposition at 450 °C using a conductive Ti/Cu support and Co−Mo catalyst system. We find that Mo stabilizes Co particles preventing lift off during the initial growth stage, thus promoting the growth of ultrahigh mass density nanotube forests by the base growth mechanism. The morphology of the forest gradually changes with growth time, mostly because of a structural change of the catalyst particles. After 100 min growth, toward the bottom of the forest, the area density decreases from ∼3−6 × 10^{11} cm^{-2} to ∼5 × 10^{10} cm^{-2} and the mass density decreases from 1.6 to 0.38 g cm^{-3}. We also observe part of catalyst particles detached and embedded within nanotubes. The progressive detachment of catalyst particles results in the depletion of the catalyst metals on the substrate surfaces. This is one of the crucial reasons for growth termination and may apply to other catalyst systems where the same features are observed. Using the packed forest morphology, we demonstrate patterned forest growth with a pitch of ∼300 nm and a line width of ∼150 nm. This is one of the smallest patterning of the carbon nanotube forests to date.

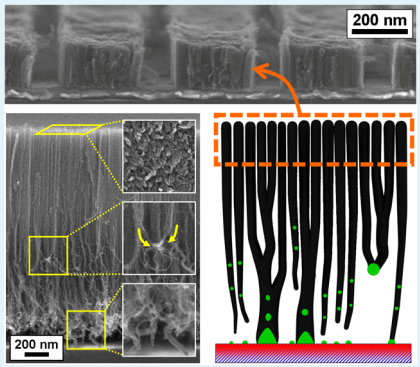

KEYWORDS: *chemical vapor deposition, low temperature growth, sputtering, Co−Mo cocatalyst, catalyst nanoparticles*

1. INTRODUCTION

Because of their outstanding structural, electrical, and thermal properties,[1−4] carbon nanotubes (CNTs) are of interest in a wide range of technologies. Vertically aligned CNT forests, in particular, are potentially the nanotube morphology to first find high-tech industrial applications such as interconnects or heat dissipation devices.[5,6] However, before realizing these applications, we need to be able to fully control the area density of the forest as well as the quality of individual tubes including diameter, number of walls, and crystallinity.

To date, chemical vapor deposition (CVD) is the only method that promises scalability at microelectronic-compatible conditions, where we have the restriction of maximum process temperature below 450 °C. Few groups have reported the low temperature growth of CNT forests in the range of 350−500 °C, whether on insulating[7] or conducting supports.[8−11] Moreover, for interconnects, we must grow the forests with high area density, with ideally 1 × 10^{13} cm^{-2} in order to exceed the properties of currently used materials such as Cu. So far, the growth of ultrahigh area density forests has been achieved only on Al_2O_3 supports,[12−14] but the area density of CNT forests on conductors tends to be lower.[15−19] Recently, Kawabata et al.[20] have reported dense vertical graphene layers, and we have shown the synthesis of ultrahigh mass density CNT forests using Co−Mo cocatalyst on Ti-coated Cu support at 450 °C.[21] Ti is used as a contact layer favoring forest growth, while keeping the conductivity between the tubes and Cu layer.[22] Mo stabilizes small Co nanoparticles on conductive supports, as shown on forest growth on insulators with Co−Mo[23,24] or Fe−Mo.[25] The diameter of the Co particles on the surface is homogeneous after annealing under NH_3 because of the strong Co−Mo−Ti chemical interaction.[21] In this paper, we report the growth kinetics of such dense forests and discuss the growth termination mechanism by systematic investigation of catalyst/support and CVD conditions. Our results show that forests change morphology during the growth, mostly because of the structural change of the catalyst nanoparticles. Throughout this process, some part of catalyst particles end up embedded within nanotubes, thus losing contact with the carbon source and causing growth termination. Finally, to show the ability of the packed forest morphology (i.e., tubes having no measurable space in between) to be patterned, we grow patterned forests with a pitch of ∼300 nm and a line width of ∼150 nm. This is one of the smallest patterning of the CNT forests to date.

2. EXPERIMENTAL SECTION

2.1. Catalyst Preparation. We use as substrate Si(100) coated with thermal oxide (200 nm) on which we deposit Cu (40 nm) and subsequently Ti (0, 3.0, or 5.0 nm). We then deposit Mo (0 or 0.8 nm) followed by Co (1.5, 2.5, or 4.0 nm), thus producing 18 catalyst

Received: June 23, 2014
Accepted: August 15, 2014
Published: August 15, 2014

combinations. In a different set of samples, we apply the combinatorial masked deposition method[26,27] to get a thickness gradient of Mo (~0.01–7.5 nm) or Co (~0.22–8.1 nm) on Ti/Cu (5.0/40 nm). All metal depositions are carried out by DC magnetron sputtering in 3.5×10^{-3} mbar of Ar. After each metal deposition, the samples are exposed to air.

2.2. CNT Growth. CNTs were grown by cold-wall thermal CVD. We first pump the CVD chamber below 6.0×10^{-2} mbar and then supply a reducing gas (H_2 or NH_3). The samples are then heated up at a rate of 3 °C s^{-1} until reaching 450 °C. At this temperature, we supply C_2H_2 to grow CNTs. We investigate four different gas conditions summarized in Table 1. The pressure is kept constant at nominal 3 mbar. After growth the heater is turned off and samples are kept under Ar until room temperature.

Table 1. Gas Flow Conditions during CVD Process

	heating up (pretreatment)			CNT growth		
	NH_3 (sccm)	H_2 (sccm)	Ar (sccm)	NH_3 (sccm)	H_2 (sccm)	C_2H_2 (sccm)
NH_3, 100%-C_2H_2[a]	200					200
H_2, 100%-C_2H_2		200				200
NH_3, 10%-C_2H_2	180		20	180		20
H_2, 10%-C_2H_2		180	20		180	20

[a]Standard CVD condition.

2.3. Catalyst System and Forest Characterization. We analyze metal supports, metal catalysts, and nanotubes forests by scanning electron microscopy (SEM, Zeiss SigmaVP, Hitachi S-5500) and transmission electron microscopy (TEM, FEI Tecnai F20). For TEM analysis, we transfer forests onto copper microgrids. We analyze the depth profiling of the metals by time-of-flight (TOF) secondary ion mass spectrometry (SIMS). We use a TOF-SIMS from ION-TOF equipped with a Bi liquid metal gun and a Cs ion gun. Bi ions are filtered for Bi_1^+ ions and Cs ions are filtered for Cs^+ ions. The sputtering raster is 250×250 μm^2 using Cs^+ at 500 eV (current 41 nA) and surface spectra are taken from an area of 50×50 μm^2 using Bi_1^+ at 25 keV (target current 0.87 pA). The guns are operated in high current bunched mode, the extractor in positive mode, and the analyzer optimized for high mass resolution, acquiring over a range from 0.5 to 740 Da. An electron flood gun is used between pulses to compensate charging effect due to insulation. During the analysis, metal-Cs clusters are followed and labeled as M^+ for the respective metal ions. The depth of the SIMS crater is measured using an optical profiling system (Wyko NT1100); it is assumed a constant sputtering rate throughout.

2.4. Density Measurement. We measure the weight of the Si substrates before (with catalyst/underlayer metals) and after the growth process using a Satorius microbalance (ME235S, readability: 0.01 mg). After the growth process, the weight gain of the Si substrates (sizes of 0.5–3.9 cm^2) with the CNT forests (0.32–2.0 μm in height) are 0.04–0.24 mg. Note that no measurable weight gain is obtained after the growth process without Co (with Mo, Ti, and Cu). From the weight gain and the volume of the forests, we obtain the mass density.[13,14] The area densities of CNTs (cm^{-2}) are obtained by two different methods. One is obtained by dividing the mass density by unit mass of CNTs,[13,14] and the other one is obtained by counting 40–400 CNTs in SEM images.

2.5. Catalyst Patterning. We sputter Mo(0.8 nm, top)/Ti(5.0 nm)/Cu(40 nm) on a Si wafer. Subsequently, poly(methyl methacrylate) is spin-coated at 5000 rpm for 40 s, giving a layer thickness of ~170 nm which is used as a resist in the lithography step. After baking at 180 °C for 2 min, the resist is patterned by exposition to an electron beam and then developed. Then, 2.5 nm of Co (catalyst) is sputtered on the developed resist and the samples are submersed in acetone and sonicated for 30 s, which dissolves the resist and lifts off the Co on the unpatterned regions. Finally, the samples are rinsed with isopropanol and dried with nitrogen before loading into the growth chamber.

3. RESULTS AND DISCUSSION

The surface growth of nanotube forests is a complex process in which each pretreatment and growth parameter influences the growth results. Employing a multimetal support/catalyst system, as we report herein, not only adds more variables to the matrix of experiments, but also enlarges the number of possible interactions. Thus, for a thorough understanding of the system, we evaluate all CVD parameters individually. In a first stage, we evaluate the 18 catalyst combinations and four CVD conditions. We present the results in the two following subsections.

3.1. Evaluation of Ti, Mo, and Co Thicknesses. Figure 1 shows the influence of each metal catalyst/support using the

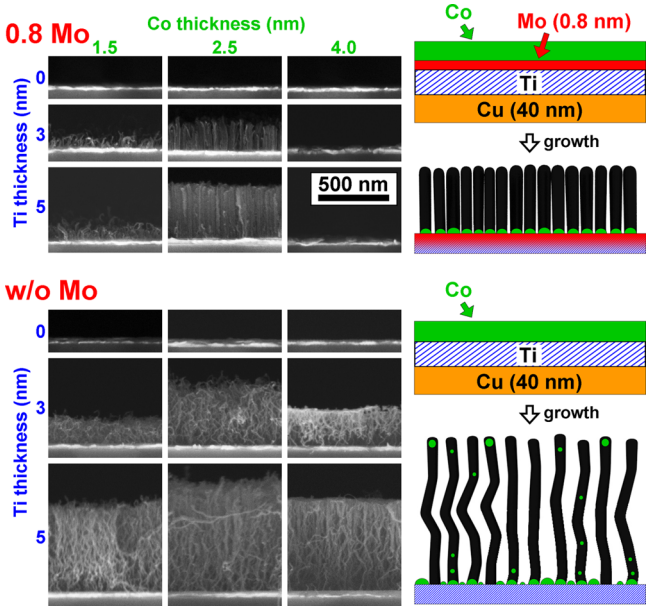

Figure 1. Side-view SEM images and schematics of the samples with different thicknesses of Ti and Co, with and without 0.8 nm Mo on Cu (40 nm) layer, grown at the standard CVD condition for 3 min. The scale bar is in common for all SEM images.

standard CVD condition for 3 min (450 °C, 200 sccm NH_3 for pretreatment, and 200 sccm C_2H_2 for growth). Side-view SEM images show that without Mo deposition, CNTs grow only when Ti is deposited in between Cu and Co. The height of the forests is enhanced by increasing the thickness of Ti. For the 2.5 nm Co case, the height of the forests increases from 0.45 μm (3.0 nm Ti) to 0.78 μm (5.0 nm Ti). Unlike 1.5 or 4.0 nm Co, the 2.5 nm thickness gives the tallest forests. The area density is $\sim 3 \times 10^{11}$ cm^{-2}, and the mass density is 0.34 g cm^{-3} with 2.5 nm Co and 5.0 nm Ti. We have previously estimated that the nucleation efficiency of the Co particles is ~35%, and found that some Co particles are embedded within the tubes.[21] The fact that Co does not catalyze the growth directly on Cu is likely to be related to both metals alloying and interdiffusing. Because of a high surface energy of Cu (1.56 J m^{-2}),[28] the catalyst metals diffuse into Cu and do not form nanoparticles. This has already been observed on Fe on Cu.[29] Diffusion is thus prevented by adding Ti and proves to be necessary also when Mo is used as cocatalyst. Using Co–Mo/Ti/Cu, the forests are

much denser and more packed compared to using only Co. For the 2.5 nm Co case, the height of the forests is 0.21 μm (3.0 nm Ti) and 0.40 μm (5.0 nm Ti). The area density is ~3−6 × 10^{11} cm^{-2} and the mass density is as high as 1.6 g cm^{-3} with 2.5 nm Co and 5.0 nm Ti. The nucleation efficiency of the Co particles is ~80%, and Co particles stay at the base of the forests.[21] The tubes are so compact that it becomes difficult to distinguish individual tubes or bundles, especially with Co/Mo (2.5/0.8 nm) on 5.0 nm Ti. Altogether, these results allow us to confirm the usefulness of Ti as interlayer on Cu, and Mo as cocatalyst for growing ultrahigh mass density CNT forests. We have confirmed ohmic behavior between the CNT forests and the Cu supports. The average measured resistance is 95 kΩ, and the lowest value is 22 kΩ.[21]

3.2. Selection of the CVD Conditions. Figure 2 shows the growth results for the four CVD conditions using only a single

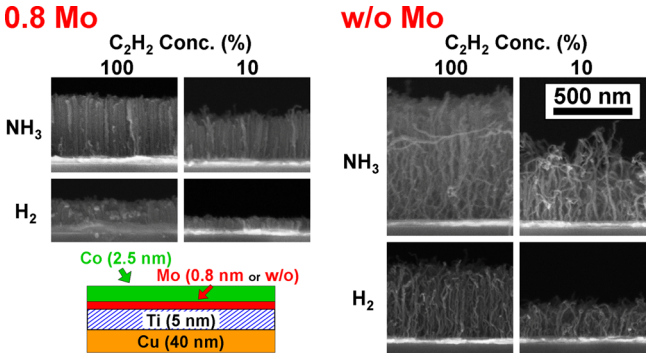

Figure 2. Side-view SEM images and a schematic of samples with and without 0.8 nm Mo. CVD is carried out at 450 °C for 3 min with different reducing gases (NH_3 or H_2) and at different C_2H_2 concentrations (100% or 10%). The catalyst/support condition is Co(2.5 nm, top)/Mo(0.8 nm or w/o)/Ti(5.0 nm)/Cu(40 nm). The scale bar is in common for all SEM images.

catalyst/support combination: Ti/Cu (5.0/40 nm) as support and Co/Mo (2.5/0.8 nm) or Co (2.5 nm) as catalyst. We observe that the forests grow taller when employing NH_3 as reducing gas during catalyst pretreatment. This might be related to the fact that the nanoparticles need to be in purely metallic state to nucleate CNTs.[30−32] At low temperatures, NH_3 proves to be more efficient than H_2 to reduce catalyst particles to its metallic state.[32] Likewise, the forests grow ~1.4−2.1 times taller with 100% C_2H_2 than with 10% C_2H_2. The forest growth appears to be limited by the diffusion of the carbon source. We note, however, that such a high concentration (100% C_2H_2) does not deactivate the catalyst particles. Although C_2H_2 is a highly reactive gas,[33−35] at 450 °C and 3 mbar total pressure, it may not produce enough amorphous carbon or other carbon impurities to poison catalyst particles.[36,37] In the following sections, all growth results are obtained using a pure NH_3 for pretreatment and 100% C_2H_2 (undiluted) for precursor (standard CVD condition in Table 1).

3.3. Combinatorial Investigation of Co and Mo Thicknesses in Optimized CVD Conditions. To investigate in detail the effect of Co/Mo thicknesses on forest growth, we prepare Co−Mo combinatorial samples on Ti/Cu (5.0/40 nm).[26,27] After preparing the Ti/Cu supports on substrates (14 × 14 mm^2), we sputter a Mo gradient (~0.01−7.5 nm) using a physical shadow mask. The samples are then rotated 90° and, following the same procedure, we deposit a Co gradient (~0.22−8.1 nm). Figure 3 shows optical images of the samples after metal sputtering (Figure 3a) and after growth (Figure 3b)

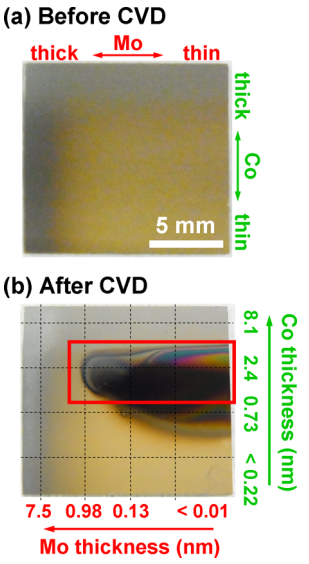

Figure 3. Optical images of combinatorial samples (a) before and (b) after CVD under the standard CVD condition for 3 min. The dotted lines in (b) are contour lines which are used to derive the thickness of Mo or Co. The scale bar in (a) is in common for (b). The area marked with a rectangle in (b) is investigated in detail in Figure 4

using the standard CVD condition for 3 min. Both Mo and Co change the thickness across the substrate position. It can be observed a region of an optimum Co/Mo thickness ratio, where CNTs nucleate and grow. When Mo is too thick (>0.98 nm), no nucleation is verified (left area of substrate), partly because of the difficulty of restructuring Co films into nanoparticles onto high-surface-energy Mo layers (2.51 J m^{-2}).[28] At the same time, the bottom area of substrate, where Mo with wide range of thickness is coated with very thin Co (<0.1 nm), no color change is observed. This indicates Mo itself does not nucleate CNTs under our CVD conditions. The thickness window in which both metals are catalytically active covers ~0.3−5 nm for Co and up to 0.98 nm of Mo. This is highlighted with a red rectangle in Figure 3b and investigated in detail in Figure 4.

Figure 4 shows an optical image of the combinatorial catalyst samples marked with rectangle in Figure 3b and corresponding side-view SEM images of the substrates after CVD. With SEM images, we show three Co thicknesses (4.0, 2.5, and 1.5 nm) for the Mo gradient (~0.01−1.9 nm). We observe two features. The forests with 2.5 nm Co grow higher in length than those at 4.0 or 1.5 nm Co under any Mo thickness. This is in agreement with growth results in Figure 1 and suggests 2.5 nm is the optimum Co thickness for the evaluated supports and CVD conditions. On the other hand, in increasing the Mo thickness (regardless of that of Co) we observe the forest height to decrease. Simultaneously, the forests become much more compact with straighter tubes. These results show the feasibility of controlling forest properties such as height and area/mass density by varying the amount of Mo as cocatalyst. The area shown with dashed rectangle in the optical image corresponds to the dense forest highlighted in SEM images in Figure 4. We find that the top-view optical image of the dense forest appear to be gray rather than black which we assume is related to the highly packed forest structure diminishing the absorbance.

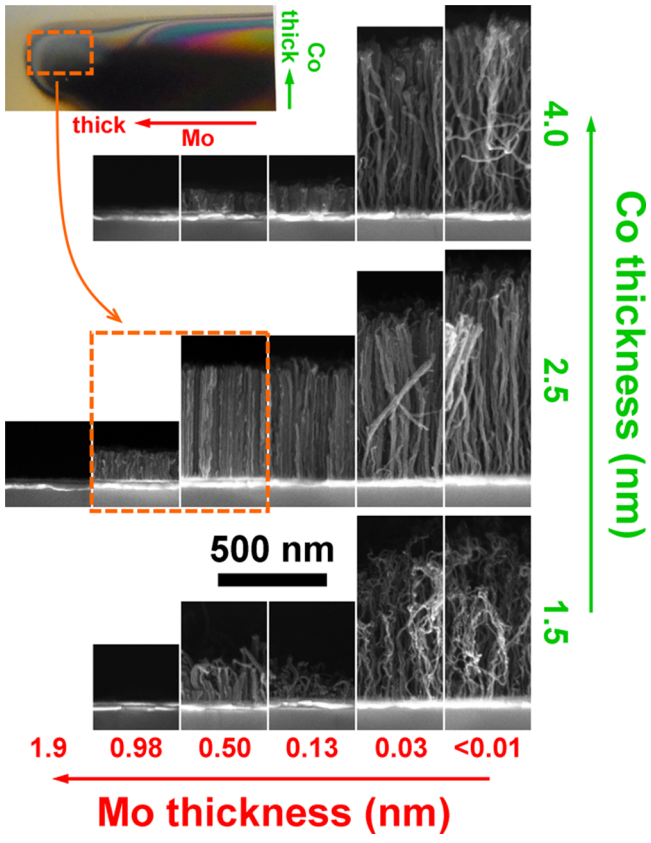

Figure 4. Optical image of the combinatorial catalyst sample marked with rectangle in Figure 3b, and corresponding side-view SEM images with Co thickness of 4.0, 2.5, and 1.5 nm on gradient Mo. The scale bar is in common for all SEM images.

3.4. TOF-SIMS. In order to investigate the state on the catalyst/support in detail, we investigate the depth profiles of the samples by TOF-SIMS. Figure 5 shows the depth profile data of 0.8 nm Mo sample before (dotted line) and after (solid line) annealing at 450 °C (Figure 5a), and with (solid line) and without (dotted line) Mo after annealing at 450 °C (Figure 5b). We can see that the oxide peaks disappeared as shown with arrows (Figure 5a) and that Mo, Ti, and Cu diffuse toward the top direction after annealing. This shows the reduction of catalyst/support and the restructuring of Co nanoparticles. The amount of Co diffusion into Ti layer appears to be nearly the same for samples with and without Mo (Figure 5b). This indicates Mo does not act as a diffusion barrier. As previously reported,[21] Mo interacts strongly both with Co and Ti, favoring the formation of uniform Co nanoparticles and also keeping the particles on the surface of the substrate during the CNT growth, hence resulting in the base growth mode of CNTs.

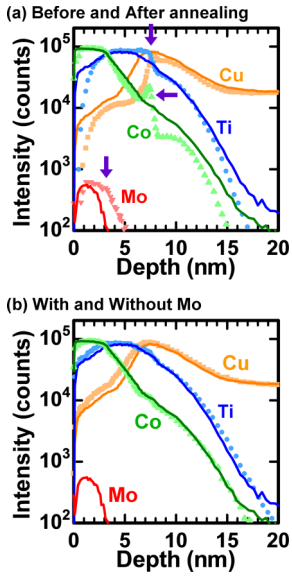

Figure 5. SIMS profiles for 0.8 nm Mo sample (a) before (dotted line) and after (solid line) annealing at 450 °C, and (b) with (solid line) and without (dotted line) Mo after annealing at 450 °C.

3.5. Growth Kinetics. In order to investigate the growth kinetics of CNT forests on Co−Mo/Ti/Cu catalyst system, we carry out CNT growth using our standard CVD condition with different growth time (3, 10, 30, and 100 min). Figures 6a - d show the side-view SEM images of the CNT forests with 0.8 nm Mo. Figure 6i shows the time evolution of both the height and the mass density of the forest with 0.8 nm Mo as well as the height evolution of the forest without Mo. The forests without Mo show a fast growth rate at the beginning of the synthesis (0.31 μm min^{-1}), and within the first 30 min they reach the plateau. In 3 min of growth the forest height is 0.92 μm, at 10 min it is 1.3 μm, and then, at 30 min growth, it is 1.5

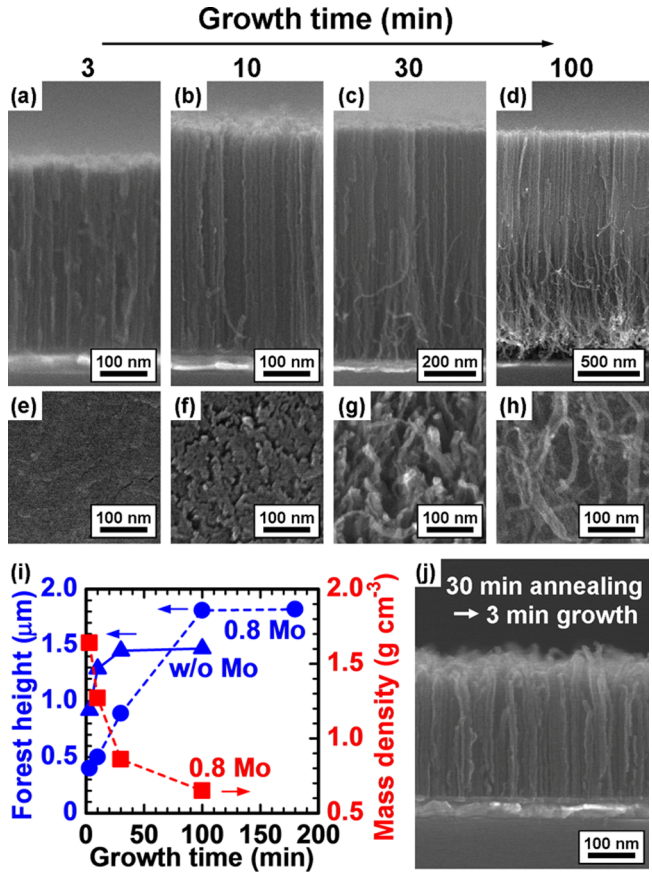

Figure 6. SEM images with (a−d) side-view and (e−h) backside-view of the forests with 0.8 nm Mo, grown at the standard CVD condition. (i) Time evolution of the forest height and mass density. (j) Side-view SEM image of the forest with 0.8 nm Mo after annealing for 30 min under NH_3 followed by 3 min growth under the standard CVD condition.

dx.doi.org/10.1021/am504048h | ACS Appl. Mater. Interfaces 2014, 6, 15440−15447

μm. It remains practically unchanged after this. In contrast, when Mo cocatalyzes the synthesis, the initial growth rate is lower than that on pure Co (0.13 μm min^{-1}). The plateau is reached at a later time (~100 min), thus implying a longer lifetime of the catalyst. The forest height is 0.40 μm in 3 min, at 10 min it is 0.50 μm, at 30 min it is 0.89 μm, and then, at 100 min growth, it is 1.8 μm. We note that, in 3 min growth, the forest with Mo shows the mass gain per unit area of 0.20 g m^{-2} min^{-1} which is double of that without Mo because of the higher mass density.[21]

We note that the dense forests keep their morphology after being transferred from the substrate to a copper grid. This allows us to examine the backside of the forests by SEM and determine the catalyst structure evolution (Figures 6e - h). We can clearly observe the structural change of catalyst layers corresponding to the side-view SEM images (Figures 6a - d). The bottom of the forests shows a progressive decrease of area density from ~3−6 × 10^{11} cm^{-2} (top part, derived from mass density and TEM images, or top-view SEM images) to ~5 × 10^{10} cm^{-2} (bottom part, derived from backside-view SEM images) with the growth time. Correspondingly, the mass density of the forest continuously decreases: 1.6 g cm^{-3} for 3 min, 1.3 g cm^{-3} for 10 min, 0.86 g cm^{-3} for 30 min, and 0.65 g cm^{-3} for 100 min, Figure 6i. These values are the averaged mass densities of the forest from top to bottom. When we focus on each time interval, the mass density is 0.61 g cm^{-3} from 3 to 10 min, 0.40 g cm^{-3} from 10 to 30 min, and 0.38 g cm^{-3} from 30 to 100 min. Unlike the morphological change of the forests reported so far,[38−41] our dense forests show more evident changes, because of their extremely packed initial morphology. We suggest this is related to the change of catalyst structure with the growth time.

A series of experiments and further characterization allows us to confirm this hypothesis. We first evaluate the effect of long annealing time (before growth), carrying out forest growth for 3 min after 30 min NH_3 annealing at growth temperature (450 °C), Figure 6j. We find that the forest morphology is very dense and similar to that obtained for short annealing times (i.e., NH_3 pretreatment only during heating up, Figure 6a). Although catalyst sintering cannot be completely ruled out during this annealing under reducing atmosphere,[42] our results clearly show the sintering is much more pronounced during the growth period.

Having excluded catalyst sintering during the pretreatment stage, we perform further SEM and TEM analysis to investigate the morphological and structural changes of the forests and individual nanotubes, respectively. Figure 7a - d show SEM and TEM images of the dense forest grown for 100 min which correspond to Figure 6d. Figure 7b and 7d are close-up images of the areas marked with dashed lines in Figure 7a and 7c, respectively. We clearly observe a significant difference between the top and bottom regions. The top region is very compact showing practically no measurable spacing between the tubes. Moving downward, the forest becomes less dense such that at the bottom the forest is composed of individual nanotubes, separated by up to tens of nanometers. We observe large diameter tubes (>20 nm) as well as small diameter ones (~7 nm) at the bottom region (arrow indications in Figure 7b). We count the tube diameter of 50 CNTs at both top and bottom regions of the forest, histograms in Figure 7. At the top region, the tube diameter presents a normal distribution (mean ± standard deviation) of 11 ± 1.7 nm (derived from top-view SEM images, upper inset in Figure 7a). At the bottom region

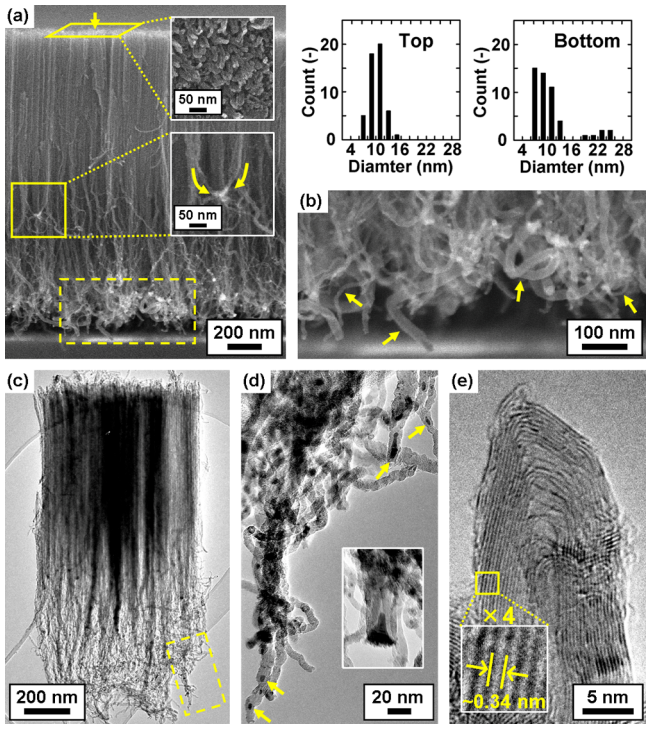

Figure 7. (a, b) Side-view SEM images with tube diameter distributions at both top and bottom part, and (c, d) TEM images of the CNT forest with 0.8 nm Mo after 100 min growth. The scale bar in (d) is the same for the inset. (e) High-resolution TEM images showing the tip of a tube.

on the other hand, the distribution is bimodal (derived from side-view SEM images, Figure 7b); about 88% of tubes have diameters of 9.6 ± 1.9 nm while nearly 12% of tubes have diameter of 23 ± 2.5 nm. In the middle of the forests, we find tubes that initially start growing more than hundreds of nanometers apart, but, due to the catalyst nanoparticles sintering, end up growing from the enlarged particle, lower inset in Figure 7a. This feature points out that seeding particles have sintered into a common catalyst particle. In Figure 7d, a large number of catalyst particles embedded within the tubes are observed (arrow indications). As observed in Figure 7b, we find some tubes with extremely large diameters due to the large particles (>20 nm) from which they grow (inset in Figure 7d). We can observe well-graphitized structures with a lattice spacing of ~0.34 nm at the tips of the tubes (Figure 7e, from 3 min growth samples), as shown in our previous paper.[21] From the whole set of observations we conclude that the changes in catalyst structures cause variations in forest morphology and nanotube structure as well as growth termination. This is fully analyzed in the following subsection.

Growth Model. We now account for the whole process of growth and termination mechanism of nanotube forests using Co−Mo/Ti/Cu catalyst system as shown in the schematics in Figure 8. CNT growth by CVD involves pretreatment of the metal catalyst for nanoparticle formation and carbon source exposure for the actual nanotube growth. During pretreatment in NH_3, both Ti/Cu and Co−Mo undergo a reduction to the metallic state (SIMS in Figure 5a). Alongside, Co films restructure into a series of nanoparticles. Under this reduction atmosphere, Co particles keep their size and density for long annealing times (e.g., 30 min, Figure 6j). The reason for this is a strong Co−Mo−Ti chemical interaction as we have

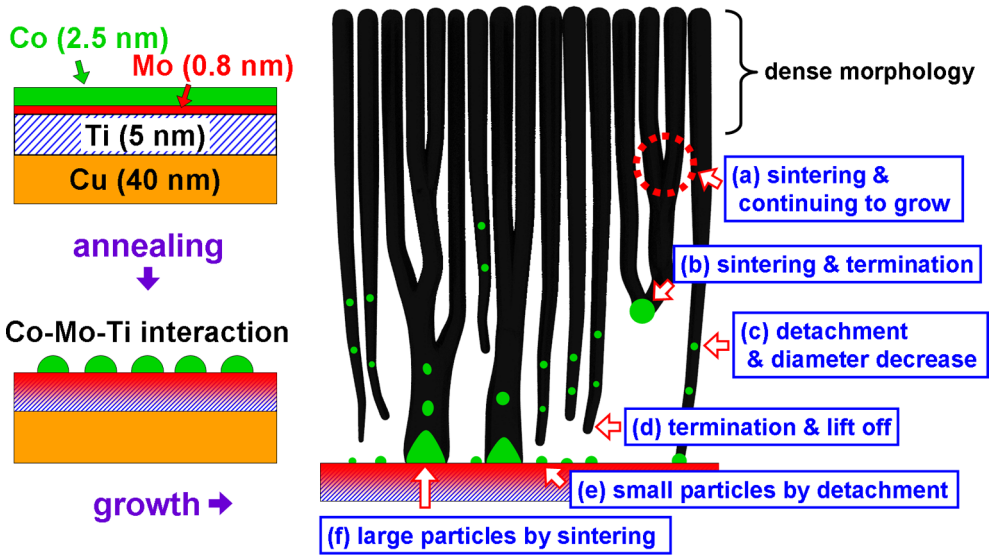

Figure 8. Schematics of CNT forest growth with Co–Mo catalyst on Ti/Cu supports. (a–f) Possible phenomena related to the growth termination.

previously reported.[21] We note that Mo does not act as a diffusion barrier (SIMS, Figure 5b). Co diffusion into the Ti layer underneath is practically the same, regardless of the presence of Mo. When the carbon source (C_2H_2 herein) is introduced, CNTs nucleate followed by the forest growth. At the initial stages, homogeneously sized Co nanoparticles nucleate extremely compact nanotube forests with high mass density of 1.6 g cm^{-3} and the area density of ~3–6 × 10^{11} cm^{-2}. Although the area density of our forests is 1 order of magnitude less than that of ultrahigh density forests achieved on Fe/Al_2O_3 (~10^{13} cm^{-2}, ~0.3–1 g cm^{-3}),[13,14] the mass density herein is ~2–5 times higher. This high mass density comes from the packed tubes with both larger diameters (e.g., ~12–13 nm) and larger wall number (e.g., ~14 walls) which are grown from relatively large catalyst particles (e.g., ~5 nm).[21] The larger diameter of the catalyst particles is due to the higher surface energy of conductive supports than that of insulating ones. Owing to the strong Co–Mo–Ti chemical interaction,[21] the Co nanoparticles remain surface bound, thus nucleating nanotubes by the root growth mechanism. However, the presence of the carbon source appears to enhance the mobility of Co catalyst. This could be related to the formation of Mo carbide weakening the Co–Mo interaction, thus leading to Co particles more mobile.[43,44] Higher metal mobility gives rise to gradual changes of the catalyst particle structure followed by the morphological change of the forest. The tube junctions indicate the migration of catalyst nanoparticles by several tens of nanometers (lower inset, Figure 7a). The migration of catalyst particles has been reported elsewhere.[45] The CNTs can either continue growing (probably at lower rates) from sintered nanoparticles with increased diameters (Figure 8a) or stop growing, after which they are lifted off by the surrounding growing CNTs (lower inset in Figure 7a, and Figure 8b). The increase of tube diameter toward the bottom of the forest is in agreement with previous reports on single-walled CNT forests.[46] On the other hand, some tubes decrease their diameters toward the bottom of the forests which leads to the bimodal diameter distribution at the bottom region (histograms in Figure 7). This tube diameter decrease can be explained as follows. As observed in TEM images (Figure 7d), some part of the particles are detached and embedded within the tubes. As a consequence, the size of remaining nanoparticles decreases followed by the tube diameter decrease, Figure 8c. When the tube diameters exceed the catalyst nanoparticle diameters, the nanoparticles are covered by the tubes and lose their catalytic activity. Once the tubes stop growing, they can be lifted off by surrounding tubes which still continue growing, Figure 8d. Note that, since the particles lose their contact with the carbon source, the detached particles do not continue catalyzing the growth.

Through the possible phenomena which include sintering, detachment, and Ostwald ripening,[27,42,47,48] (which can occur simultaneously), the catalyst nanoparticles progressively change their structure, either decreasing (Figure 8e) or increasing the diameters (Figure 8f). The diameters and densities of the forest also change, reflecting the structural change of the catalyst particles. The progressive detachment of the nanoparticles results in the depletion of the catalyst metals on the substrate surface, which is one of the critical reasons for growth termination. This growth mechanism may be the same for the growth of forests on more conventional catalysts (e.g., on Fe/Al_2O_3). The Fe/Al_2O_3 catalyst system shows the same features of nanotube density variation as well as changes in tube diameter between top and bottom of the forests.[33,38–40,46]

3.6. Growth of Patterned CNT Dense Forests. Finally, to demonstrate the ability of our packed forests to be patterned, we grow the forests with a pitch of 300–400 nm with a line width of 150–280 nm. Based on our results and growth models, in order to keep the dense forest morphology for applications, we need to intentionally stop the growth before spontaneous termination occurs. This is shown in Figure 9. Side-view SEM images illustrate the patterned forests with different dimensions. The forests show a homogeneous shape repetition across large areas of the samples (Figure 9a). We argue this is possible only because of the morphology of highly packed tubes. The smallest patterned forests have a pitch of ~300 nm with a line width of ~150 nm (Figure 9b). The morphology appears to be similar to the dense one in 3 min growth in Figure 6a. We highlight that these are one of the smallest patterned CNT forest reported thus far.

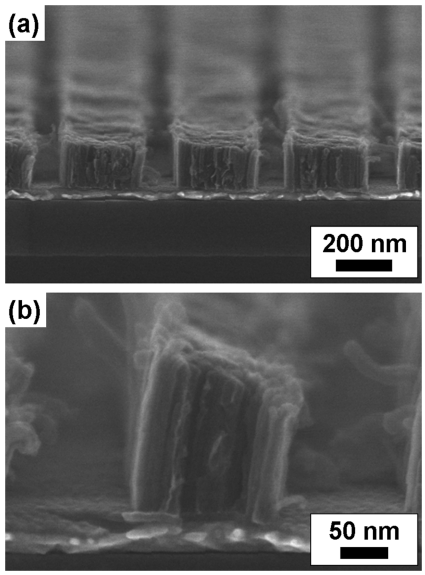

Figure 9. Side-view SEM images of patterned CNT forests. The pitch and the line width are (a) 400 and 280 nm, and (b) 300 and 150 nm, respectively.

4. CONCLUSION

We have investigated the growth kinetics and growth mechanism of ultrahigh mass density CNT forests at 450 °C. Since the forests herein are highly packed, we clearly observe the morphological changes of the forests with growth time. After 100 min growth, toward the bottom of the forest, the area density decreases from ~3−6 × 10^{11} cm^{-2} to ~5 × 10^{10} cm^{-2} and the mass density decreases from 1.6 g cm^{-3} to 0.38 g cm^{-3}. This change stems from the structural change of the catalyst nanoparticles. We observe the sintering of catalyst particles followed by the increase of the tube diameters. In addition to this, we observe a detachment of part of the catalyst nanoparticles which are embedded within the nanotubes. While these detached catalyst metals cannot catalyze the growth further as they have lost contact with the carbon source, the remaining particles grow tubes with smaller diameters. The progressive detachment of catalyst particles results in the depletion of the catalyst metals on the substrate surfaces. This is one of the crucial reasons for growth termination and may apply to other catalyst systems where the same features are observed. Using the packed forest morphology, we demonstrate patterned forest growth with a pitch of ~300 nm and a line width of ~150 nm. This is one of the smallest patterning of the CNT forests to date.

AUTHOR INFORMATION

Corresponding Author

*E-mail: hs521@cam.ac.uk.

Notes

The authors declare no competing financial interest.

ACKNOWLEDGMENTS

We acknowledge financial support from the European project GRAFOL. H.S. acknowledges a research fellowship from the Japanese Society for the Promotion of Science (JSPS). L.D. acknowledges funding from EPSRC, UK.

REFERENCES

(1) Yao, Z.; Kane, C. L.; Dekker, C. High-Field Electrical Transport in Single-Wall Carbon Nanotubes. *Phys. Rev. Lett.* **2000**, *84*, 2941−2944.

(2) Berber, S.; Kwon, Y. K.; Tomanek, D. Unusually High Thermal Conductivity of Carbon Nanotubes. *Phys. Rev. Lett.* **2000**, *84*, 4613−4616.

(3) Kim, P.; Shi, L.; Majumdar, A.; McEuen, P. L. Thermal Transport Measurements of Individual Multiwalled Nanotubes. *Phys. Rev. Lett.* **2001**, *87*, 215502.

(4) Park, J. Y.; Rosenblatt, S.; Yaish, Y.; Sazonova, V.; Ustunel, H.; Braig, S.; Arias, T. A.; Brouwer, P. W.; McEuen, P. L. Electron-Phonon Scattering in Metallic Single-Walled Carbon Nanotubes. *Nano Lett.* **2004**, *4*, 517−520.

(5) Kreupl, F.; Graham, A. P.; Duesberg, G. S.; Steinhogl, W.; Liebau, M.; Unger, E.; Honlein, W. Carbon Nanotubes in Interconnect Applications. *Microelectron. Eng.* **2002**, *64*, 399−408.

(6) Naeemi, A.; Meindl, J. D. Compact Physical Models for Multiwall Carbon-Nanotube Interconnects. *IEEE Electron Device Lett.* **2006**, *27*, 338−340.

(7) Cantoro, M.; Hofmann, S.; Pisana, S.; Scardaci, V.; Parvez, A.; Ducati, C.; Ferrari, A. C.; Blackburn, A. M.; Wang, K. Y.; Robertson, J. Catalytic Chemical Vapor Deposition of Single-Wall Carbon Nanotubes at Low Temperatures. *Nano Lett.* **2006**, *6*, 1107−1112.

(8) Shang, N. G.; Tan, Y. Y.; Stolojan, V.; Papakonstantinou, P.; Silva, S. R. P. High-Rate Low-Temperature Growth of Vertically Aligned Carbon Nanotubes. *Nanotechnology* **2010**, *21*, 505604.

(9) Nihei, M.; Kawabata, A.; Awano, Y. Direct Diameter-Controlled Growth of Multiwall Carbon Nanotubes on Nickel-Silicide Layer. *Jpn. J. Appl. Phys.* **2003**, *42*, L721−L723.

(10) Yokoyama, D.; Iwasaki, T.; Ishimaru, K.; Sato, S.; Hyakushima, T.; Nihei, M.; Awano, Y.; Kawarada, H. Electrical Properties of Carbon Nanotubes Grown at a Low Temperature for Use as Interconnects. *Jpn. J. Appl. Phys.* **2008**, *47*, 1985−1990.

(11) Nessim, G. D.; Seita, M.; O'Brien, K. P.; Hart, A. J.; Bonaparte, R. K.; Mitchell, R. R.; Thompson, C. V. Low Temperature Synthesis of Vertically Aligned Carbon Nanotubes with Electrical Contact to Metallic Substrates Enabled by Thermal Decomposition of the Carbon Feedstock. *Nano Lett.* **2009**, *9*, 3398−3405.

(12) Futaba, D. N.; Hata, K.; Yamada, T.; Hiraoka, T.; Hayamizu, Y.; Kakudate, Y.; Tanaike, O.; Hatori, H.; Yumura, M.; Iijima, S. Shape-Engineerable and Highly Densely Packed Single-Walled Carbon Nanotubes and Their Application as Super-Capacitor Electrodes. *Nat. Mater.* **2006**, *5*, 987−994.

(13) Esconjauregui, S.; Fouquet, M.; Bayer, B. C.; Ducati, C.; Smajda, R.; Hofmann, S.; Robertson, J. Growth of Ultrahigh Density Vertically Aligned Carbon Nanotube Forests for Interconnects. *ACS Nano* **2010**, *4*, 7431−7436.

(14) Zhong, G. F.; Warner, J. H.; Fouquet, M.; Robertson, A. W.; Chen, B. A.; Robertson, J. Growth of Ultrahigh Density Single-Walled Carbon Nanotube Forests by Improved Catalyst Design. *ACS Nano* **2012**, *6*, 2893−2903.

(15) Yokoyama, D.; Iwasaki, T.; Yoshida, T.; Kawarada, H.; Sato, S.; Hyakushima, T.; Nihei, M.; Awano, Y. Low Temperature Grown Carbon Nanotube Interconnects Using Inner Shells by Chemical Mechanical Polishing. *Appl. Phys. Lett.* **2007**, *91*, 263101.

(16) Yamazaki, Y.; Katagiri, M.; Sakuma, N.; Suzuki, M.; Sato, S.; Nihei, M.; Wada, M.; Matsunaga, N.; Sakai, T.; Awano, Y. Synthesis of a Closely Packed Carbon Nanotube Forest by a Multi-Step Growth Method Using Plasma-Based Chemical Vapor Deposition. *Appl. Phys. Express* **2010**, *3*, 055002.

(17) Dijon, J.; Okuno, H.; Fayolle, M.; Vo, T.; Pontcharra, J.; Acquaviva, D.; Bouvet, D.; Ionescu, A. M.; Esconjauregui, C. S.; Capraro, B.; Quesnel, E.; Robertson, J., Ultra-High Density Carbon Nanotubes on Al-Cu for Advanced Vias. In *2010 IEEE International Electron Devices Meeting (IEDM 2010)*; IEEE: Piscataway, NJ,2010; p 4.

(18) Zhang, C.; Yan, F.; Allen, C. S.; Bayer, B. C.; Hofmann, S.; Hickey, B. J.; Cott, D.; Zhong, G.; Robertson, J. Growth of Vertically-

Aligned Carbon Nanotube Forests on Conductive Cobalt Disilicide Support. *J. Appl. Phys.* **2010**, *108*, 024311.
(19) Robertson, J.; Zhong, G. F.; Esconjauregui, C. S.; Bayer, B. C.; Zhang, C.; Fouquet, M.; Hofmann, S. Applications of Carbon Nanotubes Grown by Chemical Vapor Deposition. *Jpn. J. Appl. Phys.* **2012**, *51*, 01AH01.
(20) Kawabata, A.; Murakami, T.; Nihei, M.; Yokoyama, N. Growth of Dense, Vertical and Horizontal Graphene and Its Thermal Properties. *Jpn. J. Appl. Phys.* **2013**, *52*, CB406−CB406.
(21) Sugime, H.; Esconjauregui, S.; Yang, J. W.; D'Arsie, L.; Oliver, R. A.; Bhardwaj, S.; Cepek, C.; Robertson, J. Low Temperature Growth of Ultra-High Mass Density Carbon Nanotube Forests on Conductive Supports. *Appl. Phys. Lett.* **2013**, *103*, 073116.
(22) Horibe, M.; Nihei, M.; Kondo, D.; Kawabata, A.; Awano, Y. Carbon Nanotube Growth Technologies Using Tantalum Barrier Layer for Future Ulsis with Cu/Low-K Interconnect Processes. *Jpn. J. Appl. Phys.* **2005**, *44*, 5309−5312.
(23) Murakami, Y.; Chiashi, S.; Miyauchi, Y.; Hu, M. H.; Ogura, M.; Okubo, T.; Maruyama, S. Growth of Vertically Aligned Single-Walled Carbon Nanotube Films on Quartz Substrates and Their Optical Anisotropy. *Chem. Phys. Lett.* **2004**, *385*, 298−303.
(24) Zhang, L.; Tan, Y. Q.; Resasco, D. E. Controlling the Growth of Vertically Oriented Single-Walled Carbon Nanotubes by Varying the Density of Co-Mo Catalyst Particles. *Chem. Phys. Lett.* **2006**, *422*, 198−203.
(25) Christen, H. M.; Puretzky, A. A.; Cui, H.; Belay, K.; Fleming, P. H.; Geohegan, D. B.; Lowndes, D. H. Rapid Growth of Long, Vertically Aligned Carbon Nanotubes through Efficient Catalyst Optimization Using Metal Film Gradients. *Nano Lett.* **2004**, *4*, 1939−1942.
(26) Noda, S.; Sugime, H.; Osawa, T.; Tsuji, Y.; Chiashi, S.; Murakami, Y.; Maruyama, S. A Simple Combinatorial Method to Discover Co-Mo Binary Catalysts That Grow Vertically Aligned Single-Walled Carbon Nanotubes. *Carbon* **2006**, *44*, 1414−1419.
(27) Sugime, H.; Noda, S.; Maruyama, S.; Yamaguchi, Y. Multiple ″Optimum″ Conditions for Co-Mo Catalyzed Growth of Vertically Aligned Single-Walled Carbon Nanotube Forests. *Carbon* **2009**, *47*, 234−241.
(28) Tyson, W. R.; Miller, W. A. Surface Free-Energies of Solid Metals - Estimation from Liquid Surface-Tension Measurements. *Surf. Sci.* **1977**, *62*, 267−276.
(29) Garcia-Cespedes, J.; Thomasson, S.; Teo, K. B. K.; Kinloch, I. A.; Milne, W. I.; Pascual, E.; Bertran, E. Efficient Diffusion Barrier Layers for the Catalytic Growth of Carbon Nanotubes on Copper Substrates. *Carbon* **2009**, *47*, 613−621.
(30) Nishimura, K.; Okazaki, N.; Pan, L. J.; Nakayama, Y. In Situ Study of Iron Catalysts for Carbon Nanotube Growth Using X-Ray Diffraction Analysis. *Jpn. J. Appl. Phys.* **2004**, *43*, L471−L474.
(31) Yoshida, H.; Takeda, S.; Uchiyama, T.; Kohno, H.; Homma, Y. Atomic-Scale in-Situ Observation of Carbon Nanotube Growth from Solid State Iron Carbide Nanoparticles. *Nano Lett.* **2008**, *8*, 2082−2086.
(32) Hofmann, S.; Blume, R.; Wirth, C. T.; Cantoro, M.; Sharma, R.; Ducati, C.; Havecker, M.; Zafeiratos, S.; Schnoerch, P.; Oestereich, A.; Teschner, D.; Albrecht, M.; Knop-Gericke, A.; Schlogl, R.; Robertson, J. State of Transition Metal Catalysts During Carbon Nanotube Growth. *J. Phys. Chem. C* **2009**, *113*, 1648−1656.
(33) Eres, G.; Kinkhabwala, A. A.; Cui, H. T.; Geohegan, D. B.; Puretzky, A. A.; Lowndes, D. H. Molecular Beam-Controlled Nucleation and Growth of Vertically Aligned Single-Wall Carbon Nanotube Arrays. *J. Phys. Chem. B* **2005**, *109*, 16684−16694.
(34) Zhong, G.; Hofmann, S.; Yan, F.; Telg, H.; Warner, J. H.; Eder, D.; Thomsen, C.; Milne, W. I.; Robertson, J. Acetylene: A Key Growth Precursor for Single-Walled Carbon Nanotube Forests. *J. Phys. Chem. C* **2009**, *113*, 17321−17325.
(35) Sugime, H.; Noda, S. Cold-Gas Chemical Vapor Deposition to Identify the Key Precursor for Rapidly Growing Vertically-Aligned Single-Wall and Few-Wall Carbon Nanotubes from Pyrolyzed Ethanol. *Carbon* **2012**, *50*, 2953−2960.
(36) Hata, K.; Futaba, D. N.; Mizuno, K.; Namai, T.; Yumura, M.; Iijima, S. Water-Assisted Highly Efficient Synthesis of Impurity-Free Single-Waited Carbon Nanotubes. *Science* **2004**, *306*, 1362−1364.
(37) Yamada, T.; Maigne, A.; Yudasaka, M.; Mizuno, K.; Futaba, D. N.; Yumura, M.; Iijima, S.; Hata, K. Revealing the Secret of Water-Assisted Carbon Nanotube Synthesis by Microscopic Observation of the Interaction of Water on the Catalysts. *Nano Lett.* **2008**, *8*, 4288−4292.
(38) Wang, H.; Xu, Z.; Eres, G. Order in Vertically Aligned Carbon Nanotube Arrays. *Appl. Phys. Lett.* **2006**, *88*, 3.
(39) Meshot, E. R.; Hart, A. J. Abrupt Self-Termination of Vertically Aligned Carbon Nanotube Growth. *Appl. Phys. Lett.* **2008**, *92*, 113107.
(40) Bedewy, M.; Meshot, E. R.; Guo, H. C.; Verploegen, E. A.; Lu, W.; Hart, A. J. Collective Mechanism for the Evolution and Self-Termination of Vertically Aligned Carbon Nanotube Growth. *J. Phys. Chem. C* **2009**, *113*, 20576−20582.
(41) Hasegawa, K.; Noda, S. Real-Time Monitoring of Millimeter-Tall Vertically Aligned Single-Walled Carbon Nanotube Growth on Combinatorial Catalyst Library. *Jpn. J. Appl. Phys.* **2010**, *49*, 085104.
(42) Amama, P. B.; Pint, C. L.; McJilton, L.; Kim, S. M.; Stach, E. A.; Murray, P. T.; Hauge, R. H.; Maruyama, B. Role of Water in Super Growth of Single-Walled Carbon Nanotube Carpets. *Nano Lett.* **2009**, *9*, 44−49.
(43) Herrera, J. E.; Balzano, L.; Borgna, A.; Alvarez, W. E.; Resasco, D. E. Relationship between the Structure/Composition of Co-Mo Catalysts and Their Ability to Produce Single-Walled Carbon Nanotubes by Co Disproportionation. *J. Catal.* **2001**, *204*, 129−145.
(44) Herrera, J. E.; Resasco, D. E. Loss of Single-Walled Carbon Nanotubes Selectivity by Disruption of the Co-Mo Interaction in the Catalyst. *J. Catal.* **2004**, *221*, 354−364.
(45) Kim, S. M.; Pint, C. L.; Amama, P. B.; Hauge, R. H.; Maruyama, B.; Stach, E. A. Catalyst and Catalyst Support Morphology Evolution in Single-Walled Carbon Nanotube Supergrowth: Growth Deceleration and Termination. *J. Mater. Res.* **2010**, *25*, 1875−1885.
(46) Hasegawa, K.; Noda, S. Diameter Increase in Millimeter-Tall Vertically Aligned Single-Walled Carbon Nanotubes During Growth. *Appl. Phys. Express* **2010**, *3*, 045103.
(47) Hasegawa, K.; Noda, S. Moderating Carbon Supply and Suppressing Ostwald Ripening of Catalyst Particles to Produce 4.5-Mm-Tall Single-Walled Carbon Nanotube Forests. *Carbon* **2011**, *49*, 4497−4504.
(48) Sakurai, S.; Nishino, H.; Futaba, D. N.; Yasuda, S.; Yamada, T.; Maigne, A.; Matsuo, Y.; Nakamura, E.; Yumura, M.; Hata, K. Role of Subsurface Diffusion and Ostwald Ripening in Catalyst Formation for Single-Walled Carbon Nanotube Forest Growth. *J. Am. Chem. Soc.* **2012**, *134*, 2148−2153.